Geotech Geol Eng (2008) 26:387–398
DOI 10.1007/s10706-008-9176-5

ORIGINAL PAPER

Equivalent Continuum Simulations of Geocell Reinforced Sand Beds Supporting Strip Footings

G. Madhavi Latha · Sujit Kumar Dash · K. Rajagopal

Received: 22 May 2006 / Accepted: 31 January 2008 / Published online: 20 February 2008

Abstract This paper presents an equivalent continuum method for simulating the behaviour of geocell reinforced sand foundation beds, using finite element technique. An equivalent composite model is used for numerically simulating the improvement in the strength and stiffness of sand confined with geocells. Shear strength of geocell encased sand is derived from the additional confining pressure due to geocell using hoop tension theory. The stiffness of geocell encased sand is represented by an empirical equation in terms of the stiffness of the unreinforced sand and the tensile modulus of the geocell material. Numerical simulations of strip footings resting on sand bed are carried out with and without geocell layer, varying parameters like, the dimensions of geocell layer, pocket size, depth of placement of geocell layer and the tensile modulus of the geocell material. The results of numerical analyses are validated with the corresponding experimental results. The comparison between the numerical results and the experimental results is found to be reasonably good. Some significant observations on the mechanism of geocell reinforcement have been presented in this paper.

Keywords Composite model · Geocell reinforcement · Sand bed · Strip footing · Finite element analysis · Model tests

G. Madhavi Latha (✉)
Department of Civil Engineering, Indian Institute of Science, Bangalore 560012, India
e-mail: madhavi@civil.iisc.ernet.in

S. K. Dash
Department of Civil Engineering, Indian Institute of Technology Guwahati, Guwahati 781039, India
e-mail: sujit@iitg.ernet.in

K. Rajagopal
Department of Civil Engineering, Indian Institute of Technology Madras, Chennai 600036, India
e-mail: gopalkr@iitm.ac.in

1 Introduction

Using cellular geosynthetic layers called *geocells* to reinforce soils through confinement is a relatively new technique in the field of soil reinforcement. Geocells are three dimensional, polymeric, honeycomb-like structure of cells interconnected at joints. Unlike planar reinforcements, geocells provide all-round confinement that reduce lateral spreading of the in-fill soil and thereby increase the overall rigidity of the reinforced foundation bed. Because of this relatively rigid nature of geocell mattress, the footing loads are spread over a much wider area leading to overall improvement in the behaviour. The geocell layer intercepts the potential failure planes and its rigidity forces them deeper into the foundation soil leading to higher bearing capacities.

The concept of cellular confinement of soil was first brought out by Rea and Mitchell (1978). During the last

three decades, the beneficial use of geocell reinforcement in the area of geotechnical engineering has been reported by several researchers e.g. Bathurst and Jarrett (1989); Bush et al. (1990); Cowland and Wong (1993); Bathurst and Knight (1998); Rajagopal et al. (1999); Krishnaswamy et al. (2000); Madhavi Latha (2000); Dash et al. (2001); Sitharam et al. (2005).

The finite element analysis of geocell reinforced soils requires truly 3-dimensional models because of the all round confinement of soil by geocell pockets. The geocell walls can be represented using membrane type elements in such analyses. However, the generation of meshes for such analysis would be extremely cumbersome because of the complex geometry of geocells. Hence, it would be preferable to work with equivalent 2-dimensional models that can represent the 3-dimensional nature of the geocell reinforcement. Madhavi Latha (2000) proposed an equivalent composite model for representing the strength and stiffness of geocell confined sands. This model accounts for the aspect ratio of geocell pockets, modulus of the geosynthetic used for fabricating the geocell, properties of in-fill soil etc. In this paper, this model is implemented in a finite element program for investigating the performance of strip footings resting on geocell reinforced sand beds. Results from finite element analyses are compared with the observations from model tests on strip footing resting on geocell reinforced sand bed.

2 Equivalent Composite Model for Geocell Encased Sand

Madhavi Latha (2000) proposed an equivalent composite model for geocell encased sand based on triaxial tests on sand encased in single and multiple geocells made of different geosynthetics. These triaxial tests are described in detail by Rajagopal et al. (1999). Later Rajagopal et al. (2001) validated the equivalent composite model using experiments on geocell supported model embankments constructed over soft clay bed. A brief description of the model is presented below for completeness.

2.1 Equivalent Shear Strength of Geocell Mattress

Various investigators have reported that the geocell confinement of sands induces apparent cohesion while the friction angle of the soil remains constant, Bathurst and Karpurapu (1993), Rajagopal et al. (1999). The induced cohesion in the soil is related to the increase in the confining pressure on the soil due to the geocell reinforcement through the following equation

$$c_r = \frac{\Delta\sigma_3}{2}\sqrt{K_p} \tag{1}$$

in which $\Delta\sigma_3$ is the increase in the confinement due to the geocell. The increase in the confinement due to geocell can be obtained using membrane correction theory proposed by Henkel and Gilbert (1952), which is based on the hoop tension theory, treating the geocell encased soil as a thin cylinder subjected to internal pressure. The value of $\Delta\sigma_3$ from this theory can be related to the modulus of the geocell material, equivalent diameter of the geocell pocket and the strain level.

If the volume of the soil sample remains constant during the test, the relation between the original diameter of the sample (d_o), diameter at any axial strain (d') and the corresponding axial strain (ε_a) can be derived as follows by comparing the initial volume and volume after application of strain,

$$\frac{\pi}{4}d_o^2\, L_o = \frac{\pi}{4}d^2\, L \tag{2}$$

$$\therefore d = \frac{d_o}{\sqrt{L/L_o}} = \frac{d_o}{\sqrt{1-\varepsilon_a}} \tag{3}$$

in which "L_o" is the initial length and "L" is the length of the sample at an axial strain of ε_a. Then the circumferential strain (ε_c) can be calculated as

$$\varepsilon_c = \frac{\pi d' - \pi d_o}{\pi d_o} = \frac{d' - d_o}{d_o} = \frac{1-\sqrt{1-\varepsilon_a}}{\sqrt{1-\varepsilon_a}} \tag{4}$$

Then the additional confining pressure due to the membrane stresses can be written as (Henkel and Gilbert 1952),

$$\Delta\sigma_3 = \frac{2M\varepsilon_c}{d'}\frac{1}{(1-\varepsilon_a)} = \frac{2M}{d_o}\left[\frac{1-\sqrt{1-\varepsilon_a}}{1-\varepsilon_a}\right] \tag{5}$$

where ε_a is the axial strain at failure, ε_c is the corresponding circumferential strain in the geocell, d_o is the initial diameter of individual cell pocket and d' is the diameter of the cell pocket at an axial strain ε_a. M is the modulus of the geocell material from load-strain tests corresponding to an axial strain equal to the circumferential strain measured in the geocell

(ε_c), which gets stretched in circumferential direction through hoop tension mechanism during loading.. The d_o is taken as the equivalent diameter (d) of the geocell pocket opening.

$$\begin{Bmatrix} \Delta\sigma_x \\ \Delta\sigma_y \\ \Delta\sigma_{xy} \\ \Delta\sigma_z \end{Bmatrix} = \frac{3B_t}{9B_t - E_t} \begin{bmatrix} 3B_t + E_t & 3B_t - E_t & 0 & 3B_t - E_t \\ 3B_t - E_t & 3B_t + E_t & 0 & 3B_t - E_t \\ 0 & 0 & E_t & 0 \\ 3B_t - E_t & 3B_t - E_t & 0 & 3B_t + E_t \end{bmatrix} \begin{Bmatrix} \Delta\varepsilon_x \\ \Delta\varepsilon_y \\ \Delta\gamma \\ \Delta\varepsilon_z \end{Bmatrix} \tag{7}$$

2.2 Equivalent Stiffness Properties of Geocell Mattress

The equivalent stiffness of geocell encased soil is related to the stiffness of unreinforced soil, secant modulus of geocell material and interaction parameter, which represents the interaction in case of multiple cells. The following nonlinear equation is proposed to express the Young's modulus parameter of geocell-reinforced sand (K_r) in terms of the secant modulus of the geocell material and the Young's modulus parameter of the unreinforced sand (K_e) by Madhavi Latha (2000).

$$K_r = K_e + 200\ M^{0.16} \tag{6}$$

The modulus parameter in the above equation corresponds to the modulus number in hyperbolic model proposed by Duncan and Chang (1970). This equation is developed by regression analysis of data from triaxial tests on single and multiple geocells made from different geosynthetics. The coefficients in Eq. (6) depend upon the type of soil and interaction between different cells in the layer. The values "200" and "0.16" are valid for medium dense sand confined in a layer of geocells, where each cell is surrounded by more than four cells. This equation for estimating the stiffness of geocell layer is validated by Rajagopal et al. (2001) and Madhavi Latha and Rajagopal (2007). The main advantage of the Eq. 6 is that for any given geocell material, the equivalent modulus number can be obtained by simply substituting the value of the modulus (M). This value of M should be obtained from the tensile load-strain response of the geocell material, corresponding to the strain that would develop in the geocells due to the design loading on the foundation bed.

3 Numerical Implementation

The incremental stress-strain relations for the geocell-confined sand are written in terms of the tangent Young's modulus (E_t) and tangent bulk modulus (B_t) as follows.

The tangent bulk and Young's modulus were determined in terms of the prevailing stress state using the following hyperbolic equations as proposed by Duncan et al. (1980).

$$E_t = \left[1 - \frac{R_f(1-\sin\phi)(\sigma_1 - \sigma_3)}{2c\cos\phi + 2\sigma_3\sin\phi}\right]^2 K_e P_a \left(\frac{\sigma_3}{P_a}\right)^m$$
$$B_t = K_b P_a \left(\frac{\sigma_3}{P_a}\right)^n \tag{8}$$

The various variables in the above equation are as follows; c, ϕ are the shear strength parameters of the soil, K_e and K_b are the Young's modulus and bulk modulus numbers, m and n are the corresponding exponents, P_a is the atmospheric pressure and R_f is the ratio between the failure and maximum stresses. The Poisson's ratio at any stage (μ_t) is computed in terms of the tangent moduli as follows

$$\mu_t = \frac{1}{2}\left(1 - \frac{E_t}{3B_t}\right) \tag{9}$$

The Poisson's ratio value was allowed to vary between 0.3 and 0.49 by controlling the B_t values as required. When the Poisson's ratio value exceeds 0.49, the B_t value is set to 16.667 E_t and when its value becomes less than 0.30, B_t value is set to 0.833 E_t. E_t at any strain level is determined following the procedure reported by Duncan and Chang (1970) based on the data from triaxial compression tests. It was noticed that while the Young's modulus parameter (K_e) changed with the type of geocell material and the number of pockets, the bulk modulus parameters remained relatively constant. It was observed that the K_e value for the geocell encased sand is related to the modulus of the geocell material (M) in a highly

nonlinear manner and was also found to depend on the number of geocell pockets used in the test.

The above constitutive model for geocell encased soils was implemented in a general purpose two-dimensional finite element program, called GEOFEM (Geotechnical Finite Element Modeling). This program was originally developed by Rajagopal and Bathurst (1993) at the Royal Military College of Canada, Kingston. The computer program has been validated for many geotechnical problems by Rajagopal and Bathurst (1992, 1995), Rajagopal and Sireesha (1998), Madhavi Latha (2000) and others.

The incremental equilibrium equations in this program are written in terms of the difference between the applied external forces and the equivalent nodal forces corresponding to the stresses in the previous load step (or iteration) as follows

$$[K_T]\{\delta_{ui}\} = \{P_{ext}\} - \{P_{int}\} \quad (10)$$

Where, $[K_T]$ is the tangent stiffness matrix formulated based on the stress at the beginning of the ith step and $\{\delta_{ui}\}$ is the vector of incremental displacements. $\{P_{ext}\}$ is the vector of externally applied forces at the ith step. $\{P_{int}\}$ is the vector of nodal forces corresponding to the element stresses in the previous load step and is calculated as

$$\{P_{int}\} = \int_v [B]^T \{\sigma_{i-1}\} dv \quad (11)$$

in which $[B]^T$ is the strain-displacement transformation matrix.

This scheme allows for carrying forward any out-of balance force between the external loads and the internal nodal forces corresponding to the element stresses in the previous iteration/load step, Bathe (1996). As a result, the global equilibrium is always satisfied at all stages in the analysis. With the re-applications of the imbalance force on the system, the displacements of the nodes continue to increase. As the solutions converge to the true solution, the difference between these two forces reduces and the increments of displacements also reduce. In view of the nonlinearity in the system all the analyses were performed by updating the stiffness matrix at the end of 1st iteration in every load step. The displacements were applied in small increments of 0.025 mm with several iterations at each load step, until the norms of incremental displacements and the out-of-balance forces are less than 0.5%.

In the elasto-plastic finite element analysis, the stress state predicted at the end of an increment may lie outside the current yield surface. Such discrepancies being cumulative have to be corrected back to the yield surface before the next increment of loading is applied (Nayak and Zienkiewicz 1972). In the present model, a yield surface is defined in terms of the shear strength parameters c and ϕ. A plastic potential function is defined in terms of the dilation angle (Ψ). The stress state is corrected back to the yield surface along the flow direction that is perpendicular to the plastic potential surface (Rajagopal and Bathurst 1995). This stress correction procedure will simulate the shear induced volume expansions (dilation) in the soil.

4 Laboratory Model Tests on Strip Footings

Laboratory load tests were conducted on models of strip footings placed over sand bed. A steel tank of length 1200 mm, width 332 mm and height 700 mm was used to conduct the tests on model footings. The side wall friction effects on the model tests were minimized by coating the inside of the side walls with petroleum jelly, to ensure plane strain conditions in the test tank. The model footings were made of steel and measured 330 mm × 100 mm in plan with 25 mm thickness. Uniformly graded river sand with effective particle size (D_{10}) of 0.22 mm, maximum dry unit weight (γ_{max}) of 17.41 kN/m^3 and minimum dry unit weight of (γ_{min}) of 14.30 kN/m^3 was used in these experiments. All the tests were carried out at 70% relative density of sand. The average peak angle of friction of sand at the test conditions as determined from direct shear test is 46° and from triaxial compression test is 42°. Sand pluviation technique was used to achieve uniform density in the test tank while filling the sand.

The geocells were formed using three different types of geogrids; one of these is a biaxial grid (BX) made of oriented polymer while the other two were made of non-oriented polymers, referred to as NP-1 and NP-2 grids. The properties of the geogrids were determined from standard wide width tension tests (ASTM D4595) and are listed in Table 1. The load-elongation behaviour of these geogrids is presented in

Table 1 Properties of geogrids used in tests

Property	Type of geogrid		
	BX	NP-1	NP-2
Ultimate tensile strength (kN/m)	20	4.5	7.5
Failure strain (%)	25	10	55
Initial modulus (kN/m)	183	75	95
Secant modulus at 5% strain (kN/m)	160	70	70
Secant modulus at 10% strain (kN/m)	125	45	50
Aperture size (mm)	35 × 35	50 × 50	8 × 7
Aperture opening shape	square	square	diamond

Fig. 1. The geocell mattresses were prepared by cutting the geogrids to required length and height from full rolls and placing them in transverse and diagonal directions with bodkin joints (plastic strips) inserted at the connections (Bush et al. 1990). The commonly used triangular and chevron patterns used for forming the geocells are shown in Fig. 2. In all the tests reported in this paper, chevron pattern is used to form the geocells. After preparing the geocell layer, the cells were filled with sand to a relative density of 70% using sand pluviation technique. The relative density achieved in both unreinforced zone as well as the reinforced zone (within the geocells) was ensured by measuring the in-place density through small aluminum cups of known volume placed at various locations in the test tank. The difference in relative densities measured at different locations in the test tank was found to be less than 1%.

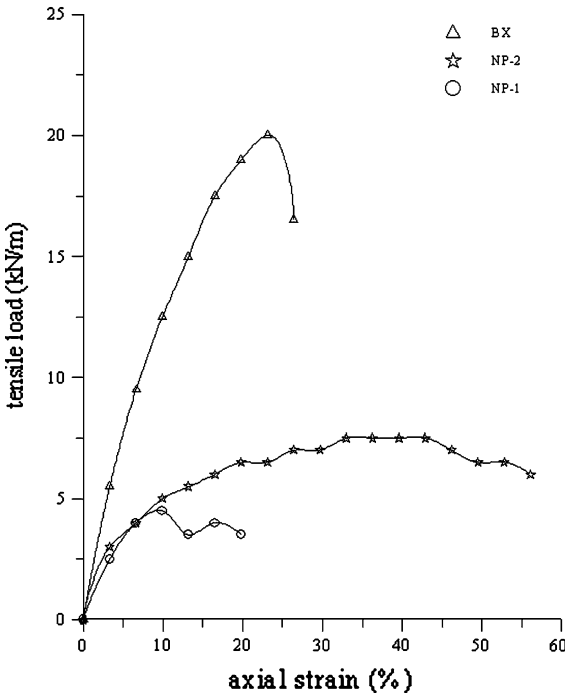

Fig. 1 Load-elongation behaviour of geogrids used in tests

The footing was placed at the center of the test tank, with the length of the footing parallel to the width of the tank. Since the length of the footing was made almost equal to the width of the tank, a plane strain condition was essentially established in the test setup. The footing was loaded through a hand operated hydraulic jack supported against a rigid reaction frame. The load on the footing was applied in small increments and each load increment was maintained constant until the footing settlement has stabilized. The settlements of the footing were measured by two dial gauges placed in diagonal directions on either side of the footing. The loading was continued until the footing settlement equals to about 50% of the footing width or till the failure whichever is earlier. The geometry of the test configurations considered in this investigation is shown in Fig. 3. The pocket size (d) of the geocells is taken as the diameter of an equivalent circular area of the geocell pocket opening, shown through hatch mark in Fig. 3 (i.e. $\frac{\pi}{4}d^2 = \frac{1}{2}d_p \times s_p$). Five series of tests were conducted by varying the pocket size of geocells (d), height of geocell layer (h), width of the geocell mattress (b), distance of the top of geocell layer below the footing (u) and type of geogrid used to form the geocell.

In addition to the vertical settlements, the circumferential strains in the geocell walls were measured during the tests by mounting strain gauges in the horizontal direction. These strain gauges could effectively measure the strains in geocells until the vertical displacement of the footing is less than about 30% of its width, s/B $<$ 30%. Beyond that, the strain gauges became inactive due to damage. At that stage, the average circumferential strain was found to be of the order of 2.5%. The corresponding axial strain was computed as 4.8% using the Eq. 4, which relates the axial and circumferential strains. This average strain value was used while estimating the increase in the confining pressure on the soil due to geocell encasement as described in a later section.

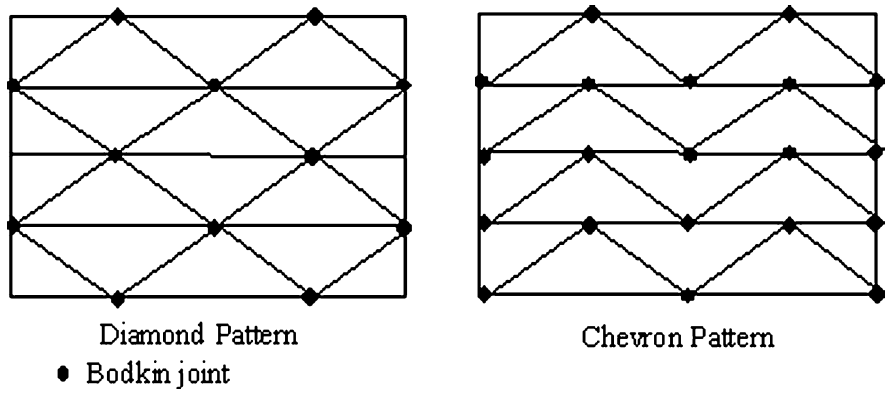

Fig. 2 Patterns used for the formation of geocells

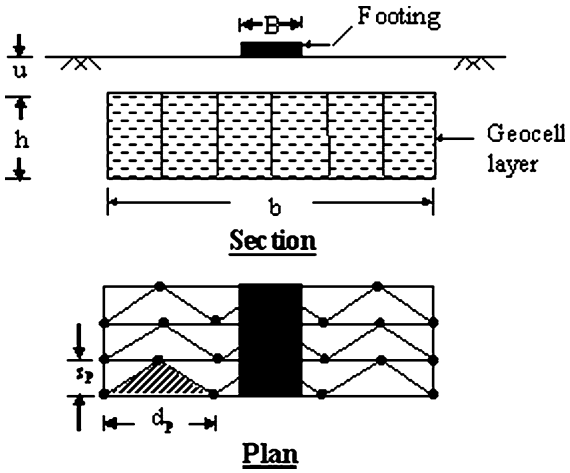

Fig. 3 Geometry of the test configuration

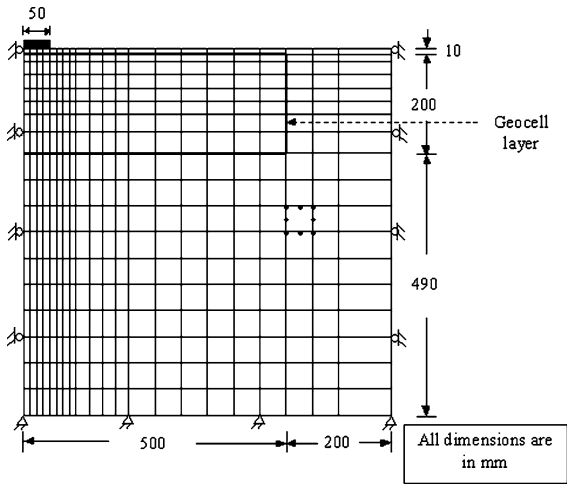

Fig. 4 Typical finite element mesh used for the analysis

5 Finite Element Analyses

The laboratory model tests described in the previous section were numerically simulated in finite element analyses. A typical mesh used for the numerical simulations is shown in Fig. 4. It consists of 1213 nodal points and 378 eight-node quadrilateral elements. All the finite element matrices (load, stiffness, reaction loads etc.) were numerically evaluated using 2×2 reduced integration order. Nagtegaal et al. (1974), Rajagopal and Sireesha (1998) have reported good success in using this type of element for accurate estimation of the limit loads of plane strain problems. As the footing is symmetric about the vertical axis at mid-section of the footing, all the finite element analyses in this investigation were carried out on half the footing by enforcing symmetry boundary conditions on the nodes along the axis of symmetry. All the boundary conditions are shown in Fig. 4. The rigidity of the footing was simulated by imposing equal vertical displacement at all the nodes corresponding to the footing. Roughness of the base of the footing was simulated by constraining the nodes on the footing from moving in the lateral direction. The reaction forces developed at the footing nodes in the vertical direction were used to compute the pressure developed in the soil at different settlement levels.

The geocell layers were modeled as equivalent composite layers with enhanced stiffness and shear strength properties, Tables 2 and 3. The friction angle of the composite layer was assumed to be equal to that of the unreinforced soil from direct shear tests consistent with the plane strain idealization of the problem. The stiffness and apparent cohesion of this layer was computed using the properties of the geocell and the infill soil. From model tests it is observed that the average circumferential strain developed in the geocells under footing loading is of the order of 2.5%.

Table 2 Equivalent stiffness parameter (K_r) for different geocell layers

Type of geogrid used to form geocells	Initial modulus of geogrid M (kN/m)	Modulus number K_r
Unreinforced	–	490
BX	183	950
NP-1	75	889
NP-2	95	904

Table 3 Apparent cohesive strength for different geocell layers

Type of geogrid	Iinitial modulus M (kN/m)	Angle of internal friction (ϕ_t^o)	Equivalent geocell pocket size d (m)	Apparent cohesion c_r (kPa)
BX	183	42.2	0.12	88
BX	183	42.2	0.15	70
BX	183	42.2	0.27	39
NP_1	75	42.2	0.15	29
NP_2	95	42.2	0.15	36.5

The corresponding axial strain is computed as 4.8% using the relation between the axial and circumferential strains (Eq. 4). The modulus 'M' of the geocell material (i.e. geogrid in the present case) is taken as the secant modulus at 2.5% stain. The dilation angle (ψ) of the soil was obtained as the slope of the graph between the vertical and horizontal deformations in the direct shear tests as 20°.

The values of K_e, m and R_f for the sand used in the present study are 490, 0.64 and 0.85 respectively as obtained from laboratory triaxial tests. The average bulk modulus number (K_b) and the exponent (n) were found to be 570 and 0.35 respectively.

6 Results and Discussion

6.1 Pressure-Settlement Behaviour

The predicted pressure-settlement responses for different cases of geocell reinforcement are compared with the corresponding observations from model tests in Figs. 5–9. In order to have a direct comparison, the responses for unreinforced sand bed are also shown in these figures.

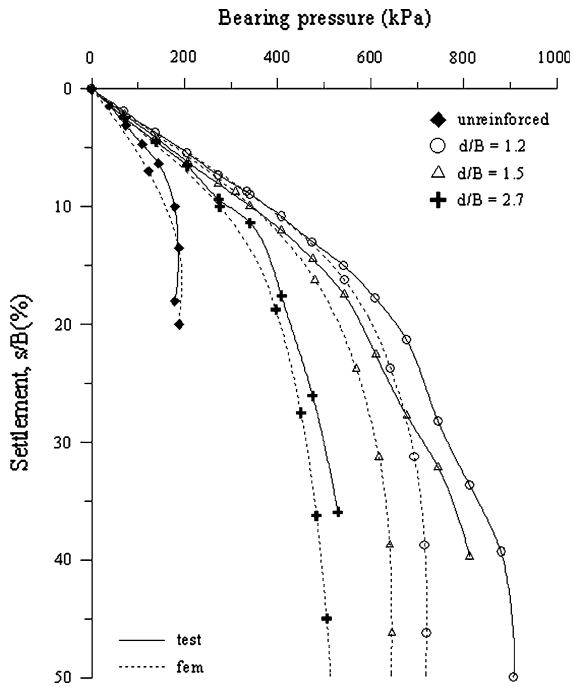

Fig. 5 Variation of bearing pressure with footing settlement for different pocket sizes of geocell (h/B = 0.8, b/B = 12, u/B = 0.1, BX-grid)

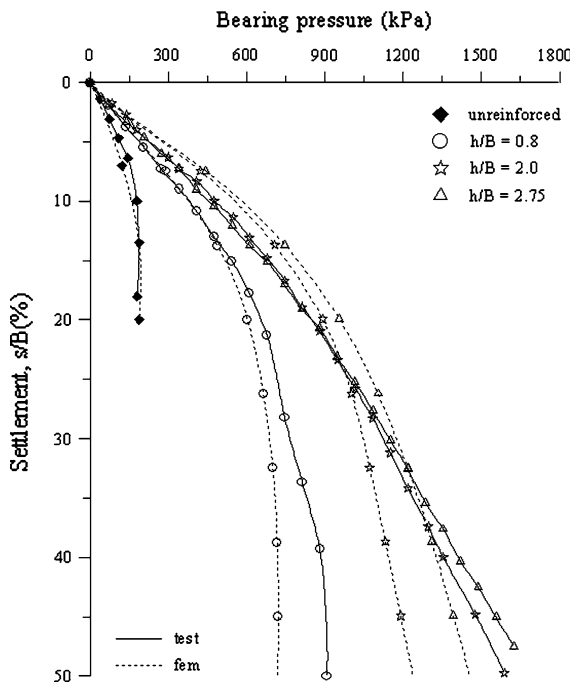

Fig. 6 Variation of bearing pressure with footing settlement for different heights of geocell mattress (d/B = 1.2, b/B = 12, u/B = 0.1, BX-grid)

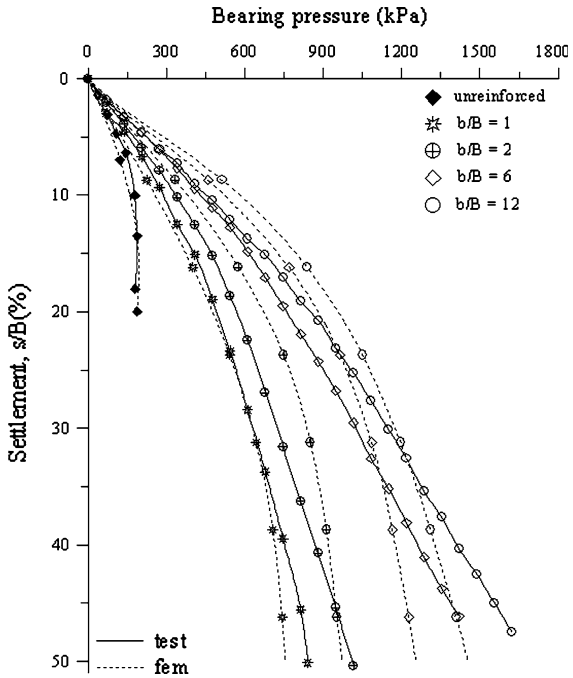

Fig. 7 Variation of bearing pressure with footing settlement for different widths of geocell mattress (d/B = 1.2, h/B = 2.75, u/B = 0.1, BX-grid)

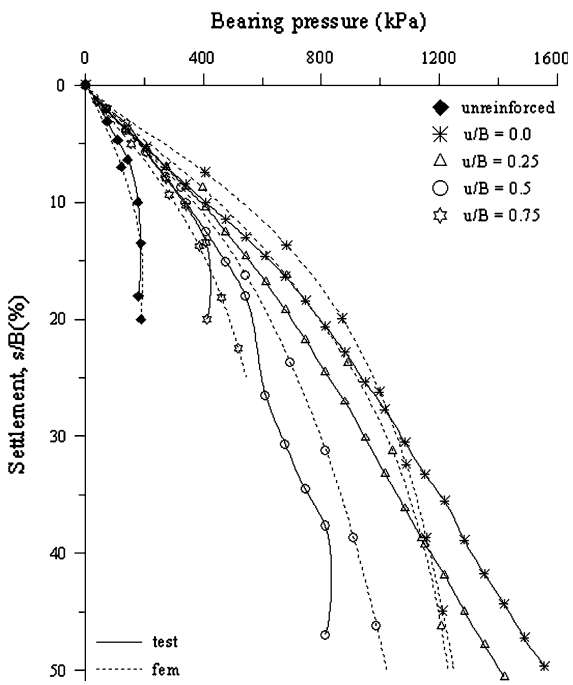

Fig. 8 Variation of bearing pressure with footing settlement for different depths of placement of geocell mattress (d/B = 1.2, h/B = 2.75, b/B = 8, BX-grid)

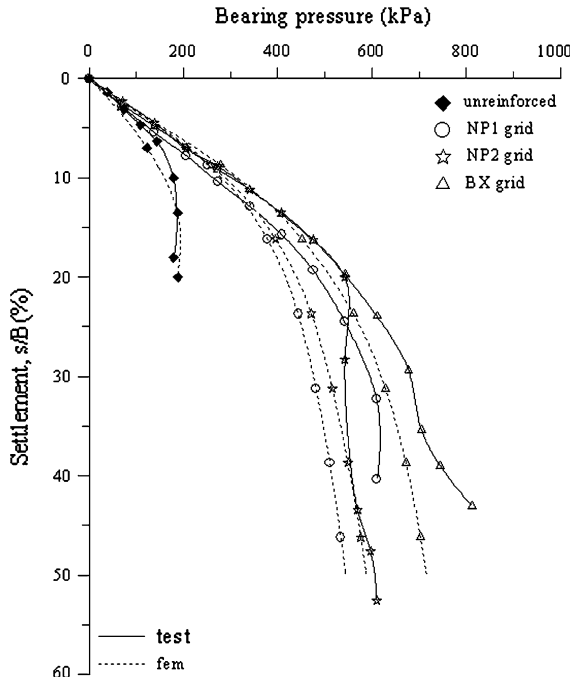

Fig. 9 Variation of bearing pressure with footing settlement for different types of geocell material (d/B = 1.5, h/B = 1.2, b/B = 8, u/B = 0.1)

The finite element predictions show a reasonably good match with the experimental ones. For geocell mattress of smaller height (i.e. h/B = 0.8) the agreement between the experimental and the predicted results is excellent up to a moderate stage of loading. The predicted responses are found to diverge from the experimental results only in the final stages of loading (Fig. 6). But as the height of geocell layer increased, the predicted pressure settlement responses have shown a little stiffer behaviour in the early stages of loading. The probable reason for this could be attributed to the fact that the apparent cohesion for geocell layer has been calculated at 2.5% circumferential strain in geocells. Since, this value is kept constant throughout the analysis; in the early stages of loading the actual strain in the geocells being lower than this (i.e. 2.5%) the analysis uses a higher mobilised strength of geocell reinforcement leading to a stiffer response. This behaviour becomes more pronounced with the increase in height of geocell mattress, where due to the deep beam effect, the shear resistance and hence cohesion plays a vital role. In the final stages of loading, the numerical predictions are on the conservative side i.e. the finite element

predicted pressures are always lower than those determined through laboratory tests. This is because, at this stage, the axial strain and hence the hoop strain developed in the geocell wall is expected to be higher than what has been used for the calculation of equivalent properties of the geocell layers (i.e. $\varepsilon_c = 2.5\%$). Such an underestimation of the strength parameters might have given rise to under prediction of results in the final stages of loading. However, the average responses predicted are found to be in good agreement with the experimentally observed values. To obtain a more exact prediction, the variation of equivalent strength parameters of the geocell layer with the strain mobilized in the geocell wall should be incorporated in the analysis.

6.2 Displacement Field

The total displacement vectors at 20% footing settlement for the unreinforced case are shown in Fig. 10. The same for the case with geocell reinforcement of b/B = 10 and b/B = 1 are shown in Figs. 11 and 12 respectively. The flow pattern in case of unreinforced sand bed shows severe lateral deformation near ground surface indicating general shear mode of failure. Besides, the displacements are found to be confined mostly in the top region. However, for the case with geocell mattress of

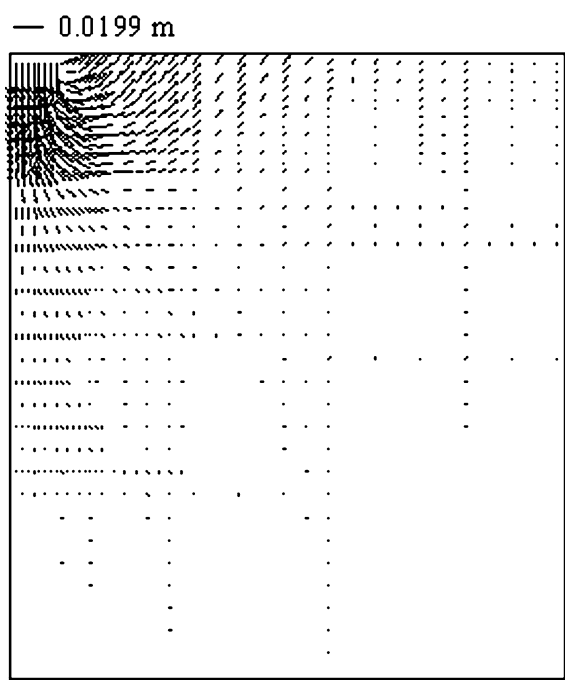

Fig. 10 Displacement vectors for the unreinforced sand bed

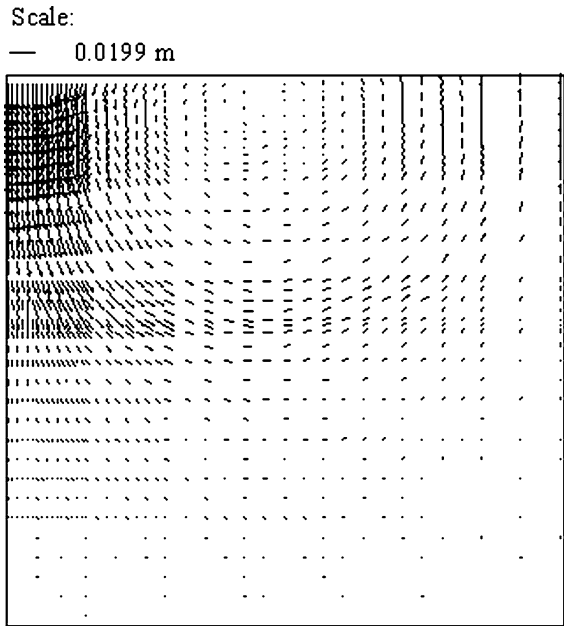

Fig. 11 Displacement vectors for the geocell reinforced sand bed (d/B = 1.2, b/B = 10, h/B = 2.75, u/B = 0, BX-grid)

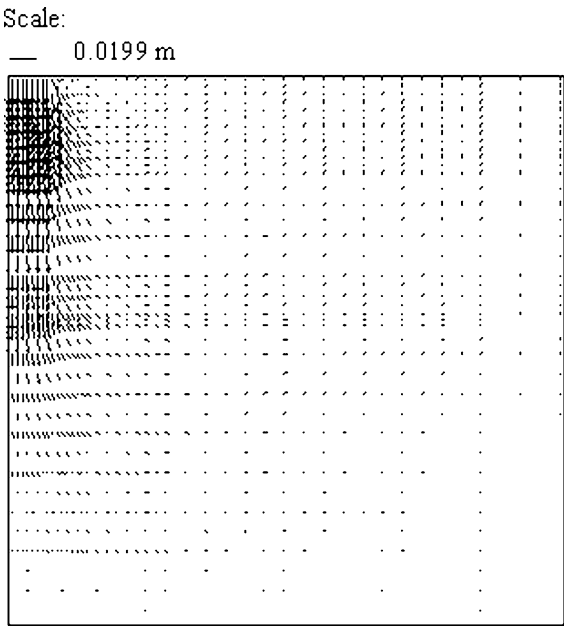

Fig. 12 Displacement vectors for the geocell reinforced sand bed (d/B = 1.2, b/B = 1, h/B = 2.75, u/B = 0, BX-grid)

b/B = 10, the lateral flow near the ground surface is found to be totally arrested and significant deformations have taken place in the subgrade soil. This finding proves that, the geocell mattress, by virtue of its rigidity, arrests the potential failure planes and forces them deeper down thereby, bringing about a higher load carrying capacity.

It is interesting to observe in the case with b/B = 1 (Fig. 12) that the flow vectors are mostly vertical with very little lateral flow. This response clearly shows that the footing load is transmitted to the foundation soil at depth just as in deep footings. Even a surface footing in this case acts like an embedded footing. As the footing loads are transferred to the soil at a deeper depth, the bearing capacity increases due to the surcharge effects.

6.3 Contours of Mobilized Shear Stress

The ratio between the shear stress and the shear strength gives valuable information on the load dispersal capacity of geocells. The value of this ratio ranges from 0 to 1 depending on the degree of mobilization of the shear strength. The value of one represents the failure of the soil. Figure 13 shows the mobilized shear stress contours for unreinforced sand bed at 20% footing settlement (i.e. s/B = 20%). Figure 14 depicts the same at 20% footing displacement with geocell mattress of width 10 times the width of the footing (b/B = 10). The bold lined rectangle in Figure 14 shows the boundary of the geocell mattress.

In case of unreinforced soil, the contours show value of 1 near the ground surface, which means that the full shear strength of the soil has been mobilized and failure has taken place. However, for the case with geocell reinforcement (b/B = 10) these values are of the order of 0.5 to 0.35. Besides, the contours of the same mobilized shear stress are generally seen to shift downwards in the reinforced case in comparison to the unreinforced one. It is also observed that in case of unreinforced sand the mobilized shear stress contour lines are normally inclined upwards towards the ground surface, away from the centerline of the footing. Whereas, below the geocell mattress they are found to be mostly horizontal indicating that, the geocell mattress settles as a rigid body. Besides, the stress contours in the region of geocell mattress are of marginal value. These findings establish the strengthening of the soil brought about by the geocell

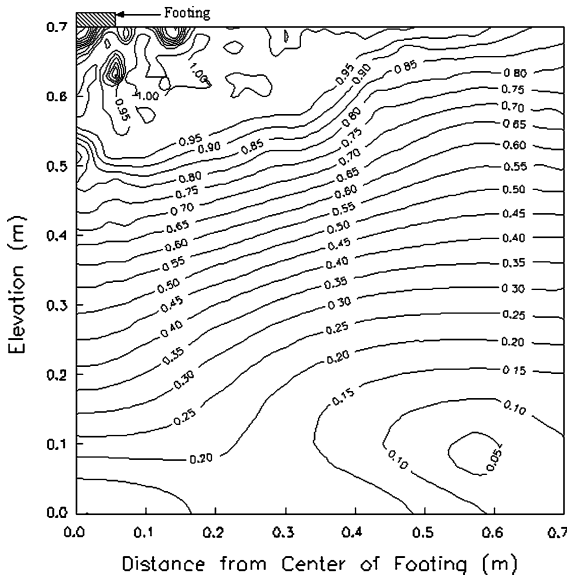

Fig. 13 Mobilized shear stress contours for unreinforced sand bed

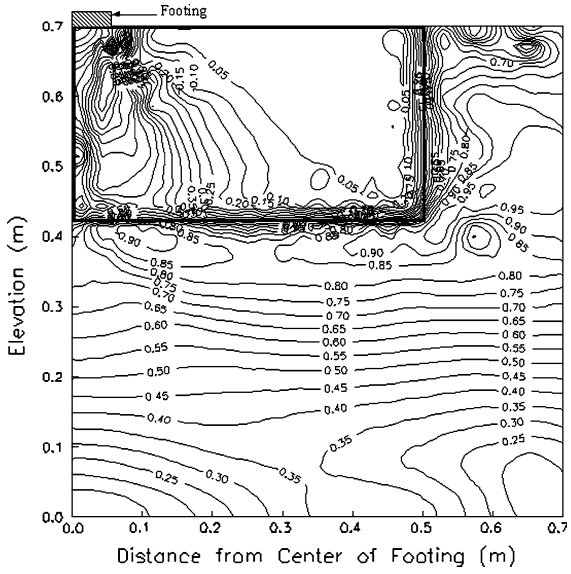

Fig. 14 Mobilized shear stress contours for geocell reinforced sand bed (b/B = 10, d/B = 1.2, h/B = 2.75, u/B = 0.1, BX-grid)

reinforcement. The contours of mobilized shear stress ratio for the case with b/B = 1 are shown in Fig. 15. Once again, the soil within the geocell region has very small contour values. The soil just adjacent to the geocell is stressed to relatively higher magnitudes because of shear stresses transmitted through the

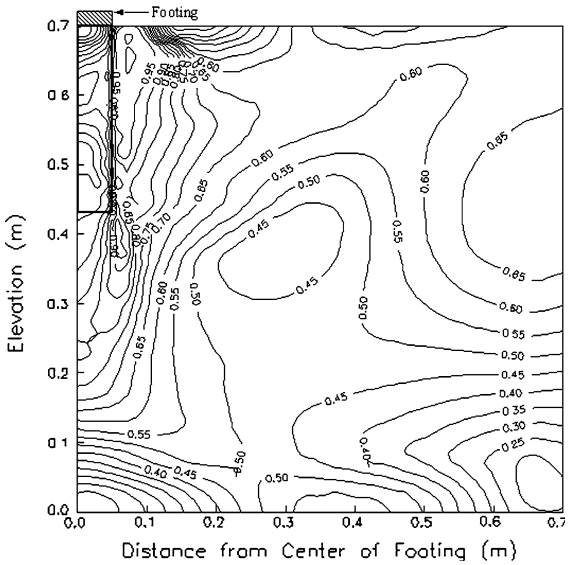

Fig. 15 Mobilized shear stress contours for geocell reinforced sand bed (b/B = 1, d/B = 1.2, h/B = 2.75, u/B = 0.1, BX-grid)

sides of the geocell. Comparison of these contours with those for unreinforced sand, shows that the unreinforced case has more soil region with full shear strength mobilized than with even the case of b/B = 1.

7 Conclusions

This paper has discussed the finite element simulations of a rigid strip footings resting on geocell reinforced sand beds modeled as equivalent continuum. This composite model accounts for the material and geometric properties of the geocell, properties of the unreinforced soil etc. in simulating the three-dimensional nature of geocell-confined soil using 2-dimensional equivalent material. The results from the finite element analyses of model footings are found to be in a fairly good agreement with those from laboratory tests.

With the provision of geocell reinforcement, the lateral flow near the ground surface is found to be totally arrested and significant deformations are observed in the subgrade soil. Besides, the contours of the mobilized shear stress are generally seen to shift downwards in the reinforced case in comparison to the unreinforced one. These findings prove that the geocell mattress by virtue of its rigidity arrests the potential failure planes and forces them deeper down, thereby, bringing about a higher load carrying capacity.

References

Bathe KJ (1996) Finite element procedures. Prentice Hall of India Private Limited, New Delhi

Bathurst RJ, Jarrett PM (1989) Large-scale model tests of geocomposite mattresses over Peat subgrades, Transportation Research Record 1188. Transportation Research Board, Washington, DC, pp 28–36

Bathurst RJ, Karpurapu R (1993) Large-scale triaxial compression testing of geocell-reinforced granular soils. Geotech Testing J, ASTM 16:296–303

Bathurst RJ, Knight MA (1998) Analysis of geocell reinforced soil covers over large span conduits. Computers Geotechn 22:205–219

Bush DI, Jenner CG, Bassett RH (1990) The design and construction of geocell foundation mattress supporting embankments over soft ground. Geotextiles Geomembranes 9:83–98

Cowland JW, Wong SCK (1993) Performance of a road embankment on soft clay supported on a geocell mattress foundation. Geotextiles Geomembranes 12:687–705

Dash SK, Krishnaswamy NR, Rajagopal K (2001) Bearing capacity of strip footings supported on geocell-reinforced sand. Geotextiles Geomembranes 19(4):235–256

Duncan JM, Chang CY (1970) Non-linear analysis of stress and strain in soils. J Soil Mech Foundations Division ASCE 96:1629–1653

Duncan JM, Byrne P, Wong KS, Mabry P (1980) Strength stress-strain and bulk modulus parameters for finite element analyses of stresses and movements in soil masses. Report No. UCB/GT/80-01, Department of Civil Engineering, University of California, Berkeley, California

Henkel DJ, Gilbert GC (1952) The effect of rubber membranes on the measured triaxial compression strength of clay samples. Geotechnique 3:20–29

Krishnaswamy NR, Rajagopal K, Madhavi Latha G (2000) Model studies on geocell supported embankments constructed over soft clay foundation. Geotech Testing J ASTM 23:45–54

Madhavi Latha G (2000) Investigations on the behaviour of geocell supported embankments. Ph.D. thesis submitted to Indian Institute of Technology Madras, Chennai

Madhavi Latha G, Rajagopal K (2007) Parametric finite element analyses of geocell supported embankments. Can Geotech J 44(8):917–927

Nagtegaal JC, Parks DM, Rice JR (1974) On numerically accurate finite element solutions in the fully plastic range. Computer Methods Appl Mech Eng 4:153–177

Nayak GC, Zienkiewicz OC (1972) Elasto plastic stress analysis, generalisation for various constitutive relations including strain softening. Int J Numerical Anal Methods Eng 5:113–134

Rajagopal K (1998) Users Manual for the Finite Element Program GEOFEM. Indian Institute of Technology Madras, India

Rajagopal K, Bathurst RJ (1992) Numerical investigation of controlled yielding of soil-retaining wall structures. Geotextiles Geomembranes 11:115–131

Rajagopal K, Bathurst RJ (1993) Users manual for Geotechnical Finite Element Modelling GEOFEM. Department of Civil Engineering, Royal Military College, Kingston, Ontario, Canada

Rajagopal K, Bathurst RJ (1995) Behaviour of geosynthetic reinforced soil retaining walls using the finite element method. Computers Geotechnics 17:279–299

Rajagopal K, Sireesha G (1998) Finite element analysis of bearing capacity of soils. Proceedings of Indian Geotechnical Conference, December, New Delhi, pp 167–170

Rajagopal K, Krishnaswamy NR, Madhavi Latha G (1999) Behaviour of sand confined with single and multiple geocells. Geotextiles Geomembranes 17:171–181

Rajagopal K, Madhavi Latha G, Krishnaswamy NR (2001) Finite element analysis of embankments supported on geocell layer using composite model. In: Desai et al. (eds) Computer methods and advances in geomechanics. Balkema, Rotterdam, pp 1251–1254

Rea C, Mitchell JK (1978) Sand reinforcement using paper grid cells. ASCE Spring Convention and Exhibit, Preprint 3130, Pittsburgh, PA, April, pp 24–28

Sitharam TG, Sireesh S, Dash SK (2005) Model studies of a circular footing supported on geocell-reinforced clay. Can Geotech J 42(2):693–703